Journal of Sound and Vibration (2002) **254**(4), 621–634
doi:10.1006/jsvi.2001.4125, available online at http://www.idealibrary.com on IDEAL®

A CONCENTRATED MASS ON THE SPINNING UNCONSTRAINED BEAM SUBJECTED TO A THRUST

S.-J. YOON AND J.-H. KIM

School of Mechanical and Aerospace Engineering, College of Engineering, Seoul National University, Shin-Rim Dong, San 56-1, *Kwan-Ak Gu, Seoul* 151-742, *Korea. E-mail: jwhkim@plaza.snu.ac.kr*

(*Received* 5 *February* 2001, *and in final form* 25 *July* 2001)

The dynamic stability of a spinning unconstrained beam subjected to a pulsating follower force $P_0 + P_1 \cos \Omega t$ is analyzed. A concentrated mass is located at an arbitrary location on the beam, and the stability of the beam is studied with the mass at various locations. The beam is analyzed using the Timoshenko-type shear deformation theory with the rotary inertia. Hamilton's principle is used to derive the equations of motion, and the spinning speed of the beam with various non-dimensional parameters subjected to a pulsating follower force is investigated. The finite element method is applied to analyze the spinning beam model, and the method of multiple scales is used to investigate the dynamic stability characteristics. A pulsating follower force is applied, and then the stability regions are changed with the transitions of the stability area in many regions. The results show that the concentrated mass increases the dynamic stability of the spinning unconstrained beam subjected to a thrust. As the spinning speed of the beam is increased, the instability regions are reduced, but various slight instability regions are additionally developed.

1. INTRODUCTION

A force can be classified as conservative or non-conservative [1]. Non-conservative force has been investigated in detail by many researchers. Generally, if the force is dependent on the motion of the body, then it is called a "follower force". Structures under a pulsating follower force may undergo static instability or dynamic instability. If the two natural frequencies merge to zero, then static instability occurs. On the other hand, if the two natural frequencies coincide with each other, then dynamic instability occurs.

Beams, plates and shells subjected to a follower force have been widely investigated in various researches on the problems of dynamic stability. Beal [2] studied the dynamic stability of flexible missiles under a constant and pulsating follower force by using the Euler–Bernoulli beam theory with Galerkin's method of analysis. In his work, it was found that divergence does not occur before flutter instability. In particular, a pulsating follower force may change the stability characteristics according to the longitudinal stiffness of the missile. Wu [3] studied the relation between the critical load and the eigencurves by using the finite element method. In his work, it was found that the magnitude and location of a concentrated mass can improve the stability characteristics of a missile. Park and Mote [4] studied the effect of a concentrated mass on the critical load and the instability type of free–free beam subjected to a follower force. In addition, it was found that a concentrated mass may induce divergence without thrust control and reduce the critical load substantially. In addition, they predicted the location and magnitude of the mass that could maximize the critical magnitude of a follower force. Kim and Choo [5] considered the effect of a concentrated mass on the dynamic stability of a free–free beam subjected to a pulsating

0022-460X/02/$35.00

follower force. The finite element method and the method of multiple scales were used to analyze the time-dependent perturbation of a follower force. Sugiyama *et al.* [6, 7] investigated the dynamic stability of a cantilevered column with a rigid-body rocket motor under a thrust. Numerical and experimental results were shown to verify the importance of the magnitude and size of the concentrated mass. In addition, the experimental verification of the effect of a follower force on the vibration and stability of cantilevered columns was studied with consideration to the sub-tangential force produced by a real solid rocket motor instead of an ideally applied tangential force.

On the other hand, several studies on the dynamic stability of a completely free shell under a follower force are available in various literatures. Bismarck [8] employed a shell model to analyze the stability of structures under a follower force. In this work, he dealt with a shallow shell rather than a cylindrical shell, and treated only a constant load. Park and Kim [9, 10] investigated the dynamic stability of a completely free–free isotropic circular cylindrical shell under a follower force. It was shown that the beam-like modes of the shell under a pulsating follower force have much larger unstable regions than the other modes. In addition, they showed that the Rayleigh mode and the Love mode affect instability, and that the shell structure can be analyzed with a beam model within only a certain range of shell dimensions. Lam and Ng [11] investigated the dynamic stability of a cylindrical shell under a pulsating axial load. Simply supported shells were examined using the various thin-shell theories for the governing equations, and Bolotin's method was used for the study of the parametric resonance. In addition, Ng *et al.* [12] analyzed the parametric resonance of the spinning cylindrical shell.

Also, the dynamic stability of spinning structures around the longitudinal axis such as a shaft or an unconstrained beam has been widely investigated. A spinning body has a stabilizing effect against the directional change of the spinning axis. In a rigid body, the stabilization characteristics increase as the spinning speed is increased. On the other hand, as the flexibility of the beam is included, the stability region may vary due to the effect of elastic modes. Bauer [13] studied the natural frequency of a spinning Euler–Bernoulli beam with various boundary conditions. Numerical results showed that the natural frequencies are linearly increased with the spinning speed. Han and Zu [14], Zu and Han [15] analyzed the changes in natural frequencies and mode shapes of a spinning Timoshenko beam using the assumed mode method. It was shown that the same mode shapes occur for both the cases of forward and backward precession. Lee [16] and Lee *et al.* [17] studied the effect of spinning on the stability region for the Euler–Bernoulli beam subjected to a pulsating compressive load. They analyzed how much initial curvature and tip mass affect the change of the dynamic instability regions. Wang [18] modelled a rotating space satellite with a long flexible antenna, and studied the elastic deformations due to the free rotation of a long, thin and elastic rod with end mass by the bifurcation method. Platus [19], Khadem and Euler [20] suggested a control of spinning flexible beam model based on the Euler or Timoshenko beam theory, respectively. Kar and Sujata [21] dealt with a rotating cantilever beam with an end mass under a transverse follower parametric excitation. The extended Galerkin method and the method of multiple scales were employed to observe the influences of system parameters.

In the present study, the dynamic stability of a spinning free–free beam with a concentrated mass subjected to a pulsating follower force $P_0 + P_1 \cos \Omega t$ is analyzed, and then the effects of axial locations of the concentrated mass are studied. Hamilton's principle is used to derive the equations of motion, and the critical spinning speed of a beam subjected to a follower force with various non-dimensional parameters is investigated. Finite elements with C_0 continuity and the method of multiple scales are used to trace the dynamic instability regions of the beam.

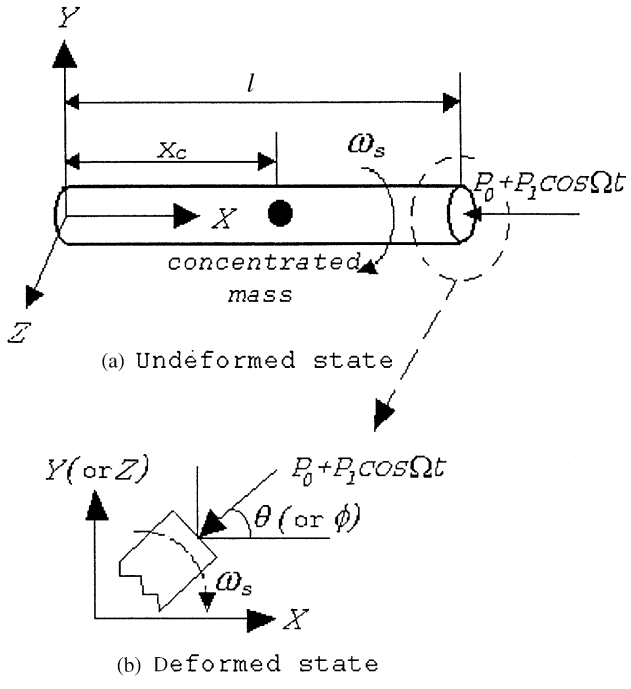

Figure 1. Spinning free–free beam with a concentrated mass subjected to a pulsating follower force.

2. FORMULATIONS

Figure 1(a) shows a spinning beam of length l with a concentrated mass M at x_0, and the spinning speed ω_s is defined in the body-fixed axis of the beam as shown in Figure 1(b). In addition, the pulsating follower force $P_0 + P_1 \cos \Omega t$ is applied at an angle θ with respect to the Z-axis and at an angle ϕ with respect to the Y-axis, and Ω denotes the driving frequency.

Displacement fields can be written as

$$u_1(x, y, z, t) = -z\phi(x, t) - y\theta(x, t), \quad u_2(x, y, z, t) = v(x, t), \quad u_3(x, y, z, t) = w(x, t), \quad (1)$$

where u_1, u_2, and u_3 are interpreted as the displacements at an arbitrary point (x, y, z). In these expressions, θ and ϕ are shear angles in the directions of the Z- and Y-axis, respectively, whereas v and w denote the deflections in the directions of the Y- and Z-axis, respectively.

Using these displacement fields, strain–displacement relationships can be written as

$$\varepsilon_{xx}(x, y, z, t) = -z\phi(x, t)_{,x} - y\theta(x, t)_{,x}, \quad \gamma_{xy}(x, y, z, t) = v(x, t)_{,x} - \theta(x, t),$$
$$\gamma_{xz}(x, y, z, t) = w(x, t)_{,x} - \theta(x, t), \quad (2)$$

where ε_{xx} is normal strain in the x direction, and γ_{xy}, γ_{xz} are shear strains in the y, z directions respectively.

Kinetic energy can be written as

$$T = \frac{1}{2}\int_0^l \rho A[\dot{v}^2 + \dot{w}^2 + \omega_s^2(v^2 + w^2) + 2\omega_s(v\dot{w} - w\dot{v})]\,\mathrm{d}x$$
$$+ \frac{1}{2}\int_0^l \rho I[\dot{\theta}^2 + \dot{\phi}^2 + 2\omega_s^2]\,\mathrm{d}x + \frac{1}{2}M[\dot{v}|^2_{x=x_c} + \dot{w}|^2_{x=x_c}] + \frac{1}{2}I[\dot{\theta}|^2_{x=x_c} + \dot{\phi}|^2_{x=x_c}], \quad (3)$$

where ρ is the mass density per unit volume, A is the cross-sectional area, and I denotes the second moment of area of the circular cross-section in the y or z direction, respectively. In addition, the overdot denotes $\mathrm{d}(\ )/\mathrm{d}t$.

Strain energy due to the bending with the shear deformations can be written as

$$U = \frac{1}{2}\int_0^l (\sigma_{xx}\varepsilon_{xx} + \tau_{xz}\gamma_{xz} + \tau_{xy}\gamma_{xy})\,\mathrm{d}V$$

$$= \frac{1}{2}\int_0^l EI[\theta_{,x}^2 + \phi_{,x}^2]\,\mathrm{d}x + \frac{1}{2}\int_0^l KGA[(v_{,x} - \theta)^2 + (w_{,x} - \phi)^2]\,\mathrm{d}x, \tag{4}$$

where $(\ )_{,\beta}$ is $\partial(\ )/\partial\beta$ ($\beta = x$ or y), K is the shear correction factor, G is the shear modulus and E is Young's modulus. In addition, EI and KGA denote the bending stiffness and the shear stiffness, respectively.

For a free–free beam, the magnitude of the follower force is distributed linearly in the neutral line of the beam due to the acceleration, and this is stated in reference [2]. In addition, as long as the exciting frequency Ω is small in comparison to the frequency of the free longitudinal vibration, the effect of the longitudinal vibration can be neglected [22].

Following these assumptions, work W_c due to the pulsating follower force $P_0 + P_1\cos\Omega t$ in the neutral line can be expressed as follows:

$$W_c = \frac{1}{2}(P_0 + P_1\cos\Omega t)\int_0^l \frac{\rho Ax + MH(x - x_c)}{\rho Al + M}(v_{,x}^2 + w_{,x}^2)\,\mathrm{d}x, \tag{5}$$

where

$$H(x - a) = \begin{cases} 1, & x > a, \\ 0, & x < a. \end{cases}$$

Virtual work of the non-conservative part of the pulsating follower force is as follows:

$$\delta W_{nc} = -(P_0 + P_1\cos\Omega t)\phi|_{x=l}\delta v - (P_0 + P_1\cos\Omega t)\theta|_{x=l}\delta w. \tag{6}$$

With these expressions, the equations of motion can be derived by the extended Hamilton's principle as

$$\delta\int_{t_1}^{t_2}(T - U + W_c)\,\mathrm{d}t + \int_{t_1}^{t_2}\delta W_{nc}\,\mathrm{d}t = 0. \tag{7}$$

3. FINITE ELEMENT METHODS AND THE METHOD OF MULTIPLE SCALES

Applying Hamilton's principle and using the finite element method, the following discretized equations of motion are obtained:

$$[\mathbf{M}]\{\ddot{X}\} + [\mathbf{G}]\{\dot{X}\} + ([\mathbf{K}_d] - \alpha P_{cr}[\mathbf{K}_f])\{X\} - \beta P_{cr}\cos\Omega t[\mathbf{K}_f]\{X\} = 0, \tag{8}$$

where

$$\{X\} = \{v_1, w_1, \theta_1, \phi_1 \ldots v_n, w_n, \theta_n, \phi_n\}^{\mathrm{T}}, \quad \alpha = P_0/P_{cr} \quad \text{and} \quad \beta = P_1/P_{cr}.$$

In these equations, $[\mathbf{M}]$ is the mass matrix, $[\mathbf{G}]$ is the gyroscope matrix due to the spinning of beam, $[\mathbf{K}_d]$ is the stiffness matrix due to the deformation of the beam, $[\mathbf{K}_f]$ is the stiffness matrix due to the follower force, and P_{cr} is the critical load. In this problem, $\{\dot{X}\}$ is the gyroscopic effect due to the spinning of the beam.

Equation (8) can be rewritten as

$$[\mathbf{M}]\{\ddot{X}\} + [\mathbf{G}]\{\dot{X}\} + [\mathbf{K}_1]\{X\} - \cos \Omega t[\mathbf{K}_2]\{X\} = 0, \tag{9}$$

where

$$[\mathbf{K}_1] = [\mathbf{K}_d] - \alpha P_{cr}[\mathbf{K}_f] \quad \text{and} \quad [\mathbf{K}_2] = \beta P_{cr}[\mathbf{K}_f].$$

Eigenvalues of these equations are the natural frequencies of the gyroscopic system, and it is supposed that four rigid-body modes (translation with respect to Y and Z directions, spinning with respect to z or y directions) can be controlled by the proper control equipment.

Equation (9) can be rewritten as follows by using the state vector $\{Y\}$ as in reference [16]:

$$\{\dot{Y}\} + [\mathbf{K}]\{Y\} = \cos \Omega t[\mathbf{F}_1]\{Y\}, \tag{10}$$

where

$$\{Y\} = \{\dot{X}, X\}^{\mathrm{T}},$$

$$[\mathbf{K}] = \begin{bmatrix} \mathbf{M}^{-1}\mathbf{G} & \mathbf{M}^{-1}\mathbf{K}_1 \\ \mathbf{I} & 0 \end{bmatrix} \quad \text{and} \quad [\mathbf{F}_1] = \begin{bmatrix} \mathbf{0} & \mathbf{M}^{-1}\mathbf{K}_2 \\ \mathbf{0} & 0 \end{bmatrix}.$$

If the system is dynamically stable, then the eigenvalues of these equations consist of conjugate pairs of pure imaginary numbers.

Equation (10) can be normalized using the modal matrix $[\mathbf{P}]$ and transformed to the following form:

$$[\mathbf{I}]\{\dot{\varsigma}\} + [\Lambda]\{\varsigma\} = \cos \Omega t[\mathbf{F}]\{\varsigma\} \tag{11}$$

where

$$\{Y\} = [\mathbf{P}]\{\varsigma\},$$

$$[\Lambda] = [\mathbf{P}^{-1}][\mathbf{K}][\mathbf{P}] \quad \text{and} \quad [\mathbf{F}] = [\mathbf{P}^{-1}][\mathbf{F}_1].$$

In addition, $[\Lambda]_i$ denotes the ith pair of $[\Lambda]$ so that

$$[\Lambda]_i = \begin{bmatrix} 0, & \Omega_i \\ -\Omega_i, & 0 \end{bmatrix}. \tag{12}$$

The transformed state vectors are introduced as follows:

$$\{\varsigma\} = \{\xi_1, \eta_1, \xi_2, \eta_2, \ldots, \xi_m, \eta_m\}^{\mathrm{T}} \quad \text{where } m = 4n. \tag{13}$$

The following equations are derived by the substitution of equation (13) into equation (11),

$$\dot{\xi}_i - \omega_i \eta_i = \sum_{j=1}^{m} (f_{2i-1,2j-1}\xi_j + f_{2i-1,2j}\eta_j) \cos \Omega t,$$

$$\dot{\eta}_i - \omega_i \xi_i = \sum_{j=1}^{m} (f_{2i,2j-1}\xi_j + f_{2i,2j}\eta_j) \cos \Omega t, \tag{14}$$

where $f_{m,n}$ is the component of $[\mathbf{F}]$.

To determine the boundaries of ξ_i and η_i for the instability regions, the method of multiple scales is used as in reference [23],

$$\xi_i(\tau) = \xi_{i(0)}(T_0, T_1, T_2) + \varepsilon\xi_{i(1)}(T_0, T_1, T_2) + \varepsilon^2\xi_{i(2)}(T_0, T_1, T_2) + \cdots$$

$$\eta_i(\tau) = \eta_{i(0)}(T_0, T_1, T_2) + \varepsilon\eta_{i(1)}(T_0, T_1, T_2) + \varepsilon^2\eta_{i(2)}(T_0, T_1, T_2) + \cdots, \tag{15}$$

where $\varepsilon(= -\beta/2)$ is the perturbation parameter.

Through first order approximation, i.e., by considering only the first two terms in equation (15), the transition curves that separate stable solutions from unstable ones in the ε–Ω plane can be defined.

Results can be summarized as follows.

Boundary of the summed-type combination resonance,

$$\Omega = \omega_p + \omega_q \pm \varepsilon\sqrt{4\Lambda_{pq}\bar{\Lambda}_{qp}}. \tag{16a}$$

Boundary of the difference-type combination resonance,

$$\Omega = \omega_p - \omega_q \pm \varepsilon\sqrt{4\Lambda_{pq}\bar{\Lambda}_{qp}}, \tag{16b}$$

where Λ_{pq} and $\bar{\Lambda}_{qp}$ are defined as

$$\Lambda_{pq} = \tfrac{1}{4}[(f_{2p,2q-1} + f_{2p-1,2q}) + i(f_{2p-1,2q-1} + f_{2p,2q})],$$

$$\bar{\Lambda}_{pq} = \tfrac{1}{4}[(f_{2q,2p-1} + f_{2q-1,2p}) + i(f_{2q-1,2p-1} + f_{2q,2p})].$$

From equations (16a) and (16b), it is easily seen that the summed-type and difference-type combination resonances cannot exist simultaneously for any pair of natural frequencies ω_p and ω_q.

4. RESULTS AND DISCUSSIONS

The non-dimensional parameters are defined as

$Q_0 = \dfrac{P_0 l^2}{EI}$ (constant part of the follower force),

$Q_1 = \dfrac{P_1 l^2}{EI}$ (pulsating part of the follower force),

$S = \dfrac{KGAl^2}{EI}$ (shear deformation parameter),

$R = \dfrac{I}{Al^2}$ (rotary inertia parameter),

$\bar{\Omega}^2 = \dfrac{\rho A l^4 \Omega^2}{EI}$ (driving frequency of the pulsating follower force),

$\bar{\omega}^2 = \dfrac{\rho A l^4 \omega^2}{EI}$ (natural frequency of the beam),

$\bar{\omega}_s^2 = \dfrac{\rho A l^4 \omega_s^2}{EI}$ (spinning rate of the beam),

TABLE 1

Comparison of magnitudes of critical follower force

	$S = 10^6$			$S = 10^3$		
	$\bar{M} = 0$ $\bar{I} = 0$	$\bar{M} = 0{\cdot}2$ $\bar{I} = 0$	$\bar{M} = 0{\cdot}2$ $\bar{I} = 10^{-3}$	$\bar{M} = 0$ $\bar{I} = 0$	$\bar{M} = 0{\cdot}2$ $I = 0$	$\bar{M} = 0{\cdot}2$ $\bar{I} = 10^{-3}$
Present	111·5	184·6	181·2	103·2	162·9	161·2
Reference [5]	111·4	181·6	177·9	102·4	161·4	159·4

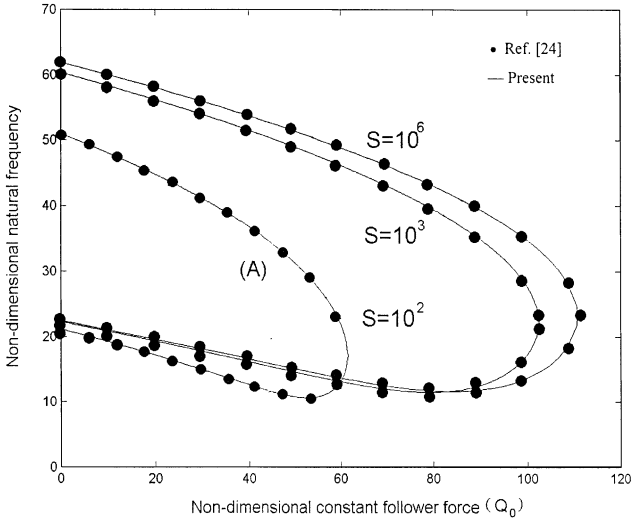

Figure 2. Effect of follower forces on a free–free Timoshenko beam.

$\bar{M} = \dfrac{M}{\rho A l}$ (mass ratio between concentrated mass and beam),

$\mu = \dfrac{x_0}{l}$ (location of concentrated mass relative to the length l).

4.1. CODE VERIFICATION

Numerical studies are performed by using the 20 three-node Lagrange elements. Validity of the numerical results in this study is checked, by comparing the critical follower force with the results of the reference. Table 1 summarizes the magnitude of the critical follower force of a free–free beam compared with those of the results in reference [5]. In the case of $S = 10^3$, where a concentrated mass is considered, 1% error of the maximum difference is observed. When $S = 10^6$, 2·7% error in the maximum difference is observed. These results indicate the validity of the code in the present study. Figure 2 shows the results for the numerical analysis of the non-dimensional natural frequency of the free–free Timoshenko beam subjected to a follower force. As shown in the figure, the results are shown to coincide with reference [24].

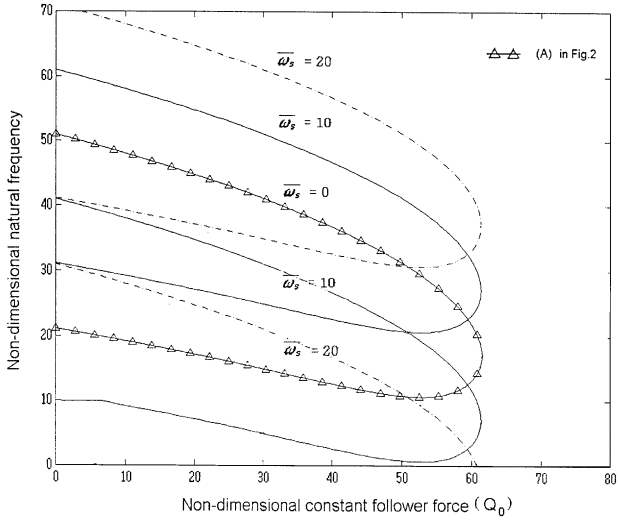

Figure 3. Eigenvalues of the spinning free–free Timoshenko beam subjected to a constant follower force.

4.2. EFFECT OF SPINNING SPEED

Now, consider the effect of spinning on the longitudinal axis of the beam subjected to a constant follower force. Figure 3 shows the eigenvalue curves of the beam for the case where the non-dimensional spinning speeds ϖ_s are 0, 10 and 20. The results indicate that the spinning speed does not change the critical value of the follower force, but does change the natural frequencies and mode shapes due to the forward and backward precession. In addition, precession results in the separation of the vibration modes can be seen in this figure. In general, spinning of a body contributes to the stability of a rigid-body mode, but it changes the instability region of the elastic mode. This is because the spinning speed does not affect the stability of the beam under the critical load, but it changes the eigenvalues and mode shapes. The case where $P_0/P_{cr}(= \alpha)$ equals 0·5 for Figures 4–6 is considered.

Figure 4 shows parametric instability regions of the spinning beam subjected to a pulsating follower force. Non-dimensional spinning speeds of the beam are chosen as 0, 10 and 20. In addition, the non-dimensional shear deformation parameter is chosen as 10^2 and the non-dimensional rotary inertia parameter R as 10^{-2}. Figure 4(a) indicates the parametric instability regions where ω_s equals to zero. In addition, this case indicates that the non-dimensional shear deformation parameter S is equal to 10^2 in Figure 3. The instability regions near $2\omega_1$, $\omega_2 - \omega_1$, $2\omega_2$ and $\omega_4 - \omega_1$ appear relatively wide, as indicated in reference [5]. As the spinning speed of the beam is increased, the instability region is reduced, that is "stabilized", as seen in Figure 4(b). As the spinning speed of the beam is increased, the tendency to stabilize becomes more apparent. The results for the case where the non-dimensional spinning speed is equal to 20 are omitted.

4.3. EFFECT OF ROTARY INERTIA AND SHEAR DEFORMATION

Figure 5 depicts the parametric instability regions of the spinning beam subjected to pulsating follower force. As the non-dimensional shear deformation parameter 10^2 is used,

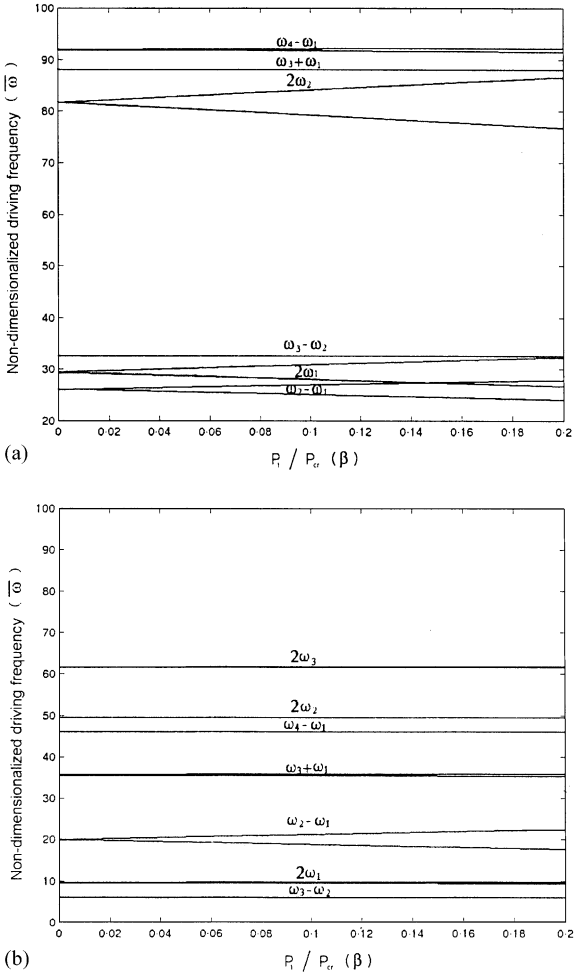

Figure 4. Parametric instability regions of the spinning beam subjected to a pulsating follower force. (a) $\bar{\omega}_s = 0$; (b) $\bar{\omega}_s = 10$.

and the non-dimensional rotary inertia parameter is set to zero. As shown in Figure 5(a), for the case in which the non-dimensional spinning speed is 10, the instability regions near $\omega_2 - \omega_1$ and $2\omega_2$ are wider than the other cases. For the case, where the non-dimensional spinning speed is 20, the instability regions near $2\omega_2$ and $\omega_3 + \omega_1$ is wider than the other instability regions, and the instability region is decreased as compared with Figure 5(a). As a result, the spinning speed of the beam is increased and the instability regions are reduced, but various instability areas are additionally developed.

4.4. EFFECT OF A CONCENTRATED MASS

In Figure 6, the effect of the location of the concentrated mass on the dynamic instability is shown. As the non-dimensional shear deformation parameter 10^2 is used, and the non-dimensional rotary inertia parameter is set to 10^{-2}. In addition, the mass ratio between the concentrated mass and beam ($\bar{M}$) is 0·2, and the non-dimensional spinning speed (ϖ_s) is 20.

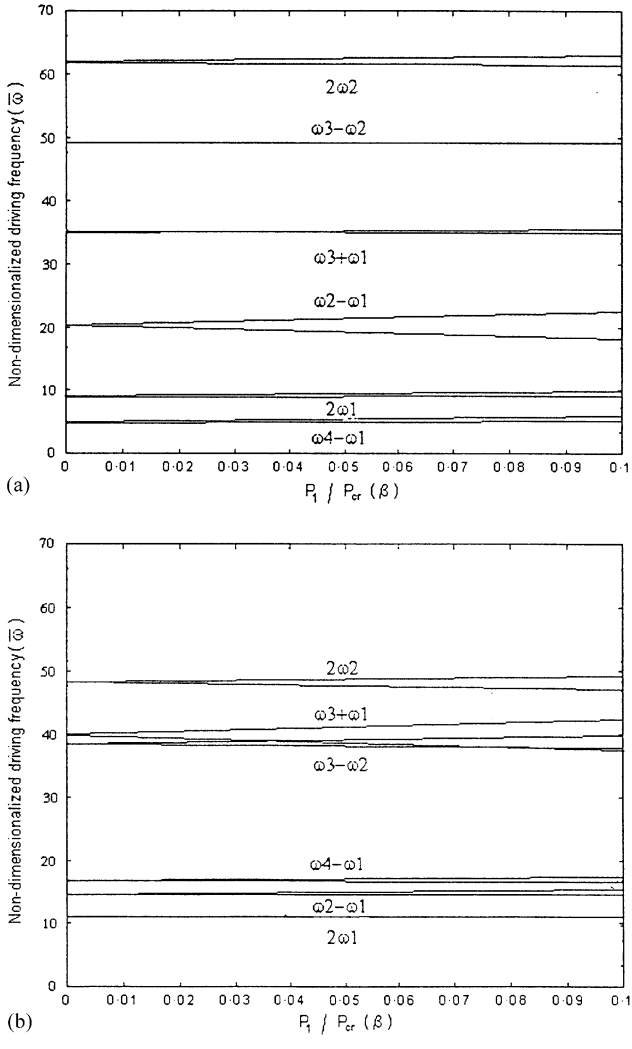

Figure 5. Parametric instability regions of the spinning beam subjected to a pulsating follower force for $S = 10^2$ and $R = 0$. (a) $\bar{\omega}_s = 10$; (b) $\bar{\omega}_s = 20$.

An instability region is observed to appear around $2\omega_2$ regardless of the location of the mass. On the other hand, other types of combination resonances are very sensitive to the location of the concentrated mass. Figure 7 describes the effect of the concentrated mass and shows the slope of the instability region near $2\omega_1$. It is easily seen that the larger the concentrated mass, the smaller the instability region. In other words, the system becomes more stable as the mass ratio is increased. In addition, Figure 8 shows the effect of the spinning speed of the beam. As the spinning speed is increased, the unstable characteristics are reduced. The dependency of the Q_{cr} at instability upon the mass M and its location μ is summarized in Figure 9. For $\mu < 0{\cdot}4$, the force at instability is decreased by addition of concentrated mass, and conversely for $\mu > 0{\cdot}4$, the critical force is increased by the addition of concentrated mass. Positioning the concentrated mass as close as possible to the thrust maximizes the stability effect.

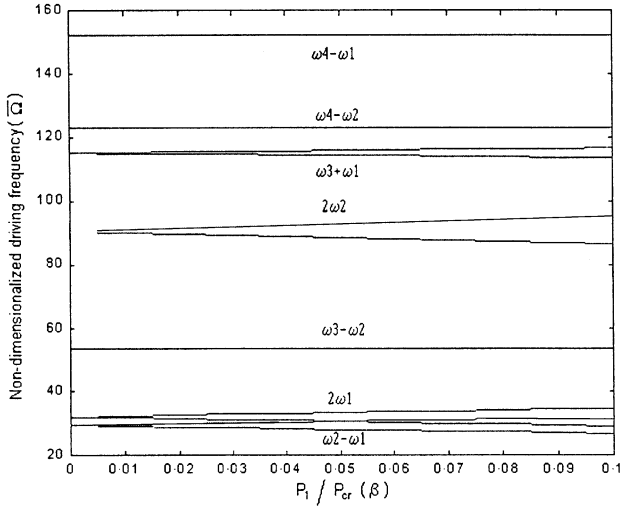

Figure 6. Parametric instability regions of the spinning beam with a concentrated mass subjected to a pulsating follower force for $S = 10^2$, $R = 0$ and $\mu = 0{\cdot}3$.

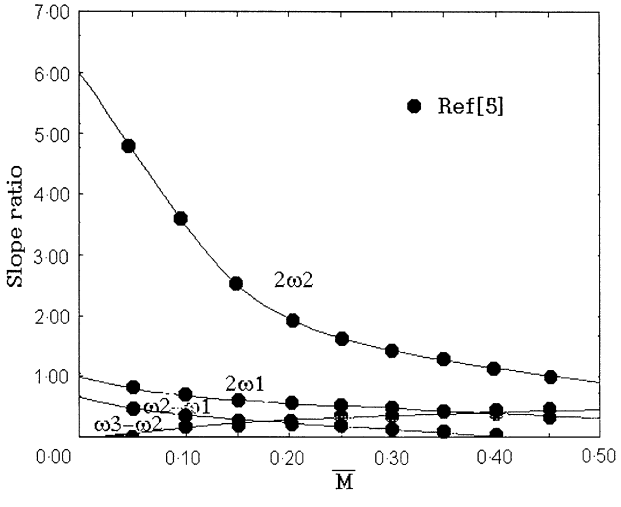

Figure 7. Effect of concentrated mass on the beam subjected to a pulsating follower force for $S = 10^3$ and $R = 3 \times 10^{-4}$.

5. CONCLUSION

The dynamic stability of a spinning unconstrained beam is investigated with a concentrated mass subjected to a pulsating follower force. The spinning beam is modelled with the Timoshenko beam theory, and the pulsating follower force is assumed to be $P_0 + P_1 \cos \Omega t$. The equations of motion are discretized by the finite element method, and the method of multiple scales is used to study the dynamic instability characteristics. Results of the analysis of the present study can be summarized as follows:

(1) The critical load of a free–free beam under a constant follower force is not affected by the spinning motion, but the natural frequency is changed.

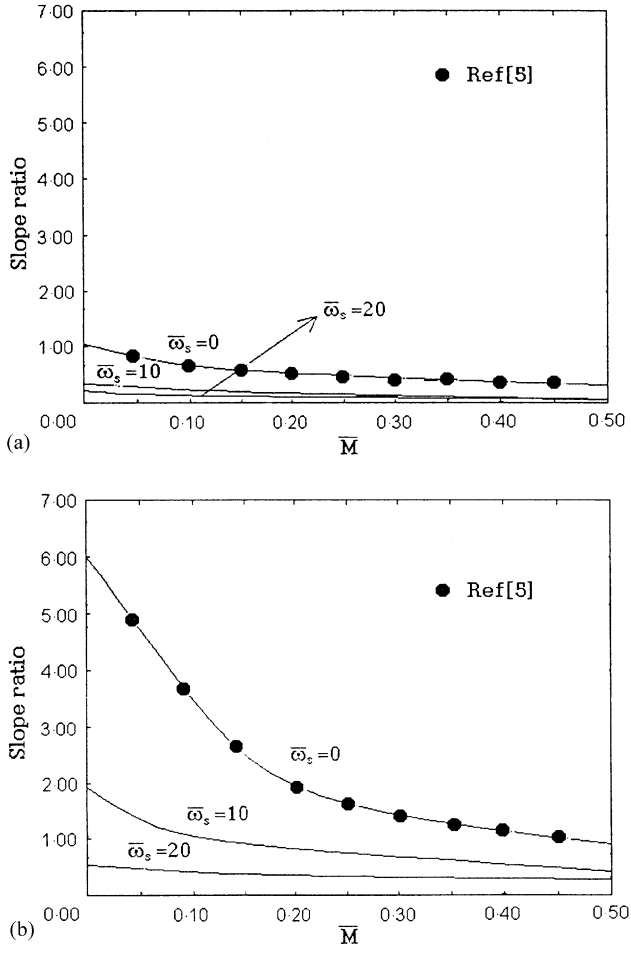

Figure 8. Effect of concentrated mass on the spinning beam subjected to a pulsating follower force for $S = 10^3$ and $R = 3 \times 10^{-4}$. (a) $2\omega_1$; (b) $2\omega_2$.

(2) The case where a pulsating follower force is applied on the spinning beam, shows instability regions, and area transitions in various regions. The reason for this is that the natural frequency characteristics change due to the spinning of the beam. For the spinning speed of the beam is increased, the instability areas of the regions are reduced, but various slight instability regions are additionally developed.

(3) The critical load Q_{cr} is changed as the rotary inertia and shear deformation are changed. The critical load is changed more rapidly with the change of shear deformation than with the change of rotary inertia. This means that shear deformation, than the rotary inertia, has more effect on the dynamic stability characteristics.

(4) The concentrated mass shows the stabilizing effect with decrease of the dynamic instability regions. The magnitude of the critical follower force is decreased (increased) monotonically, and almost linearly with the addition of concentrated mass at location $\mu < 0{\cdot}4$ ($\mu > 0{\cdot}4$). In addition, the thrust force can be maximized when the concentrated mass is positioned at the location of the thrust of the beam, $\mu = 1$.

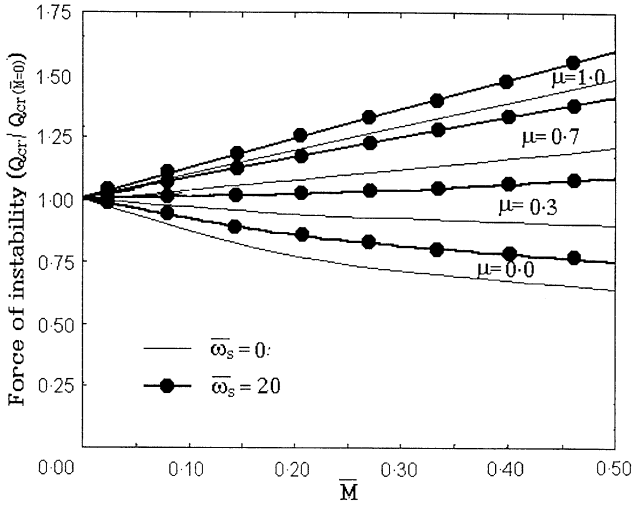

Figure 9. Force at instability of the spinning beam with a concentrated mass subjected to pulsating follower force for $S = 10^3$ and $R = 3 \times 10^{-4}$.

ACKNOWLEDGMENT

This work was supported by the Brain Korea 21 project.

REFERENCES

1. V. V. BOLOTIN 1963 *Non-conservative Problems of the Theory of Elastic Stability*. Oxford: Pergamon Press.
2. T. R. BEAL 1965 *American Institute of Aeronautics and Astronautics Journal* **3**, 486–494. Dynamic stability of a flexible missile under constant and pulsating thrust.
3. J. J. WU 1976 *American Institute of Aeronautics and Astronautics Journal* **14**, 313–319. Missile stability using finite elements—an unconstrained variational approach.
4. Y. P. PARK and C. D. MOTE 1985 *Journal of Sound and Vibration* **98**, 247–256. The maximum controlled follower force on a free–free beam carrying a concentrated mass.
5. J. H. KIM and Y. S. CHOO 1998 *Journal of Sound and Vibration* **216**, 623–636. Dynamic stability of a free–free Timoshenko beam subjected to a pulsating follower force.
6. Y. SUGIYAMA, K. KATAYAMA, K. KIRIYAMA and B. J. RYU 2000 *Journal of Sound and Vibration* **236**, 193–207. Experimental verification of stability of vertical cantilevered columns subjected to a sub-tangential force.
7. Y. SUGIYAMA, J. MATSYIKE, B. A. RYU, K. KATAYAMA, S. KINOI and N. ENOMOTO 1995 *American Institute of Aeronautics and Astronautics Journal* **3**, 499–503. Effect of concentrated mass on stability of cantilevers under rocket thrust.
8. M. N. BISMARCK 1995 *American Institute of Aeronautics and Astronautics Journal* **33**, 355–360. Dynamic stability of shallow shells subjected to follower force.
9. S. H. PARK and J. H. KIM 2000 *American Institute of Aeronautics and Astronautics Journal* **38**, 1070–1077. Dynamic stability of a free–free cylindrical shell under a follower force.
10. S. H. PARK and J. H. KIM 2000 *Journal of Sound and Vibration* **231**, 989–1005. Dynamic ability of a completely free circular cylindrical shell subjected to a follower force.
11. K. Y. LAM and T. Y. NG 1997 *Journal of Sound and Vibration* **207**, 497–520. Dynamic stability of cylindrical shells subjected to conservative periodic axial loads using different shell theories.
12. T. Y. NG, K. Y. LAM and J. N. REDDY 1998 *Journal of Sound and Vibration* **214**, 513–529. Parametric resonance of a rotating cylindrical shell subjected to periodic axial loads.
13. H. F. BAUER 1980 *Journal of Sound and Vibration* **72**, 177–189. Vibration of rotating uniform beam. Part I: Orientation in the axis of rotation.

14. P. S. HAN and J. W. ZU 1992 *Journal of Sound and Vibration* **156**, 1–6. Modal analysis of rotating shafts: a body-fixed axis formulation approach.
15. J. W. ZU and P. S. HAN 1992 *Journal of Applied Mechanics* **59**, 197–204. Natural frequencies and normal modes of a spinning Timoshenko beam with general boundary conditions.
16. H. P. LEE 1995 *Computer Methods in Applied Mechanics* **127**, 115–126. Dynamic stability of spinning pre-twisted beams subjected to axial pulsating loads.
17. H. P. LEE, T. H. TAN and G. S. B. LENG 1997 *Journal of Sound and Vibration* **199**, 401–415. Dynamic stability of spinning Timoshenko shafts with a time-dependent spin rate.
18. C. Y. WANG 1986 *Journal of Applied Mechanics* **53**, 864–868. Free rotation of and elastic rod with an end mass.
19. P. H. PLATUS 1992 *Journal of Guidance and Control* **55**, 144–151. Aeroelastic stability of slender, spinning missiles.
20. S. E. KHADEM and J. A. EULER 1992 *Proceedings of the American Institute of Aeronautics and Astronautics* **92-2211**-cp, 1224–1236. Dynamic stability of spinning flexible spinning. Part II: Vibration and stability analysis of a structurally damped controlled free–free Bernoulli–Euler beam, as a model for flexible missiles.
21. R. C. KAR and T. SUJATA 1992 *Journal of Sound and Vibration* **154**, 81–93. Stability boundaries of a rotating cantiliver beam with end mass under a transverse follower excitation.
22. V. V. BOLOTIN 1964 *The Dynamic Stability of Elastic Systems*. San Francisco, CA: Pholden-Day.
23. C. S. HSU 1963 *American Society of Mechanical Engineers Journal of Applied Mechanics* **30**, 367–372. On the parametric excitation of a dynamic system having multiple degrees of freedom.
24. Y. P. PARK 1987 *Journal of Sound and Vibration* **113**, 407–415. Dynamic stability of free Timoshenko beam under a controlled follower force.